Geosci. Model Dev., 10, 1157–1174, 2017
www.geosci-model-dev.net/10/1157/2017/
doi:10.5194/gmd-10-1157-2017

Geoscientific Model Development
Open Access
EGU

A 4D-Var inversion system based on the icosahedral grid model (NICAM-TM 4D-Var v1.0) – Part 1: Offline forward and adjoint transport models

Yosuke Niwa[1], Hirofumi Tomita[2], Masaki Satoh[3,4], Ryoichi Imasu[3], Yousuke Sawa[1], Kazuhiro Tsuboi[1], Hidekazu Matsueda[1], Toshinobu Machida[5], Motoki Sasakawa[5], Boris Belan[6], and Nobuko Saigusa[5]

[1]Oceanography and Geochemistry Research Department, Meteorological Research Institute, Tsukuba, Japan
[2]RIKEN Advanced Institute for Computational Science, Kobe, Japan
[3]Atmosphere and Ocean Research Institute, The University of Tokyo, Kashiwa, Japan
[4]Japan Agency for Marine-Earth Science and Technology, Yokohama, Japan
[5]Center for Global Environmental Research, National Institute for Environmental Studies, Tsukuba, Japan
[6]V. E. Zuev Institute of Atmospheric Optics, Russian Academy of Sciences, Siberian Branch, Tomsk, Russia

Correspondence to: Y. Niwa (yniwa@mri-jma.go.jp)

Received: 29 August 2016 – Discussion started: 11 October 2016
Revised: 6 February 2017 – Accepted: 20 February 2017 – Published: 17 March 2017

Abstract. A four-dimensional variational (4D-Var) method is a popular algorithm for inverting atmospheric greenhouse gas (GHG) measurements. In order to meet the computationally intense 4D-Var iterative calculation, offline forward and adjoint transport models are developed based on the Nonhydrostatic ICosahedral Atmospheric Model (NICAM). By introducing flexibility into the temporal resolution of the input meteorological data, the forward model developed in this study is not only computationally efficient, it is also found to nearly match the transport performance of the online model. In a transport simulation of atmospheric carbon dioxide (CO_2), the data-thinning error (error resulting from reduction in the time resolution of the meteorological data used to drive the offline transport model) is minimized by employing high temporal resolution data of the vertical diffusion coefficient; with a low 6-hourly temporal resolution, significant concentration biases near the surface are introduced. The new adjoint model can be run in discrete or continuous adjoint mode for the advection process. The discrete adjoint is characterized by perfect adjoint relationship with the forward model that switches off the flux limiter, while the continuous adjoint is characterized by an imperfect but reasonable adjoint relationship with its corresponding forward model. In the latter case, both the forward and adjoint models use the flux limiter to ensure the monotonicity of tracer concentrations and sensitivities. Trajectory analysis for high CO_2 concentration events are performed to test adjoint sensitivities. We also demonstrate the potential usefulness of our adjoint model for diagnosing tracer transport. Both the offline forward and adjoint models have computational efficiency about 10 times higher than the online model. A description of our new 4D-Var system that includes an optimization method, along with its application in an atmospheric CO_2 inversion and the effects of using either the discrete or continuous adjoint method, is presented in an accompanying paper (Niwa et al., 2016).

1 Introduction

We have developed a new four-dimensional variational (4D-Var) inversion system for estimating surface fluxes of greenhouse gases (GHGs; presently, primarily targets are carbon dioxide (CO_2) and methane (CH_4)). The new system is referred to as NICAM-TM 4D-Var, the 4D-Var inversion system based on the Transport Model version of the Nonhydrostatic ICosahedral Atmospheric Model. It consists mainly of forward and adjoint transport models and an optimization scheme. This paper presents derivation of the transport models and evaluate their performances. The accompanying pa-

per (Niwa et al., 2016) describes the optimization scheme and demonstrates the application of the new system to an atmospheric CO_2 inversion problem.

The 4D-Var inversion method has evolved over the years to achieve higher spatiotemporal resolution in inverse calculations of various atmospheric trace gas measurements (Rödenbeck, 2005; Chevallier et al., 2005; Baker et al., 2006; Meirink et al., 2008; Basu et al., 2013; Wilson et al., 2014; Liu et al., 2014) that include continuous measurements at the surface, as well as aircraft (Machida et al., 2008; Sawa et al., 2015; Matsueda et al., 2015) and satellite observations (e.g., Yokota et al., 2009). The 4D-Var method is an iterative method requiring multiple model simulations, not only forward but also backward using an adjoint model. Moreover, a global inversion calculation of an atmospheric greenhouse gas requires analysis over a long period ($\sim$20 years; e.g., Chevallier et al., 2010) to figure out interannual variations of surface fluxes, resulting in at least hundreds of years of model simulations in total. This provides strong motivation for us to develop ways of making the computations more efficient.

For GHG simulations, there are two types of atmospheric transport models: one is online (e.g., Patra et al., 2009) and the other is offline (e.g., Kawa et al., 2004; Krol et al., 2005). Online models include atmospheric general circulation models (AGCMs) which incorporate passive tracers of GHGs and simulate their movements. Offline models are those that simulate transport of tracer gases using archived meteorological data (e.g., temperature, wind velocity, and humidity). Therefore, an offline model is computationally much more efficient than an online model, and hence is favored for the 4D-Var calculation. However, archived meteorological data usually consist of reanalysis data with limited spatiotemporal resolution. Furthermore, temporal snapshots of reanalysis data are not physically consistent with each other (Stohl et al., 2004). Therefore, in offline transport calculation, reanalysis wind data should be modified in advance to restore the dynamical consistency with pressure tendencies; otherwise the tracer mass cannot be conserved (Heimann and Keeling, 1989; Heimann, 1995; Bregman et al., 2003).

An adjoint model integrates variables backward in time to calculate sensitivities of a certain scalar variable against model parameters (Errico, 1997), with applications for data assimilation and inversion analyses. Furthermore, the adjoint sensitivity is a powerful tool to diagnose tracer transport mechanisms (e.g., Vukićević and Hess, 2000). For GHG inverse analyses, the atmospheric processes are considered to be all linear, with CO_2 and CH_4 transported as passive tracers and CH_4 losses calculated by simple linear equations with prescribed hydroxyl (OH) and chlorine (Cl) radicals and $O(^1D)$ (Patra et al., 2011). However, in practice, nonlinearity is introduced into the discretized model, which complicates adjoint model formulation. One prominent example is the discretization of an advection scheme. An advection scheme with higher-than-first-order accuracy must employ a nonlinear algorithm to preserve tracer monotonicity (Godunov, 1959). Therefore, an advection scheme often uses a nonlinear flux limiter or fixer that depends on tracer quantities, introducing nonlinearity and discontinuity. However, the direct adjoint of such a nonlinear code is computationally inefficient for a long simulation, because it requires several checkpoints from which time forward simulations are restarted to restore tracer quantities at every model time step. Furthermore, it has been found that such an adjoint model is ill-behaved due to discontinuities (Thuburn and Haine, 2001; Vukićevićet al., 2001). Therefore, alternative approaches have been proposed at the expense of linearity or the accuracy of numerical scheme (Vukićević and Hess, 2000; Vukićevićet al., 2001; Sandu et al., 2005; Hourdin and Talagrand, 2006; Hakami et al., 2007; Gou and Sandu, 2011; Haines et al., 2014). Most studies use either the "discrete adjoint" or "continuous adjoint". However, which approach performs better is still controversial. The discrete adjoint is linear but reduces the accuracy of the numerical scheme, while the continuous adjoint is nonlinear but maintains the monotonicity.

In this study, we have achieved a level of computational efficiency to conduct a 4D-Var inversion of atmospheric GHGs using offline forward and adjoint models. The offline model is closely linked to the AGCM of Nonhydrostatic ICosahedral Atmospheric Model (NICAM: Tomita and Satoh, 2004; Satoh et al., 2008, 2014). In fact, the model can be considered as an offline version of the online transport model of NICAM-based Transport Model (NICAM-TM: Niwa et al., 2011a, b). In the offline model, tracer transport is calculated in the same way as in the online model, but driven by meteorological data provided from the AGCM run of NICAM in which winds fields are nudged toward reanalysis data. Compared to the reanalysis data, the physical and dynamical consistency in the nudged AGCM data is maintained. Furthermore, the use of the AGCM enables us to change the spatiotemporal resolution of the meteorological input data. Similar AGCM-based offline models have been developed by previous studies (Hourdin et al., 2006; Yumimoto and Takemura, 2013). In fact, the offline NICAM-TM has already been used in a CO_2 inversion studies using the conventional matrix calculation method (Niwa et al., 2012). In this study, we examine the relative impact of the meteorological driver data with different temporal resolutions in each of the transport processes (advection, vertical diffusion, and cumulus convection) on model accuracies. Maintaining the same degree of flexibility in the time resolution of the offline forward model, we develop a new adjoint model. The new adjoint model can be run in discrete or continuous mode. In order to achieve the exact adjoint relationship with its corresponding forward model, the discrete adjoint method switches off the nonlinear flux limiter in the advection scheme, while the continuous adjoint utilizes the flux limiter to give preference to monotonicity over the adjoint exactness.

Because thinning (i.e., reducing time resolution, resulting in a decreased number of data points) of the meteorological

data might introduce some additional model errors in the offline calculation, we evaluate those errors by comparing CO_2 concentrations simulated by the offline model with those by the online model. In that evaluation, we test various temporal resolutions of the meteorological data, which are separately determined for each transport process. Also, we validate fundamental properties of the adjoint model and demonstrate the utility of the adjoint sensitivity in a back-trajectory analysis.

2 Methods

2.1 NICAM

The horizontal grid of NICAM has a distinctive structure. Different from the conventional latitude–longitude grid models, it has a quasi-homogenous grid distribution produced from an icosahedron obtained by a recursive division method (Stuhne and Peltier, 1996). This avoids the pole problem inherent in latitude–longitude grids and facilitates global high-resolution simulations. Due to the feasibility of high-resolution simulations, the dynamical core of NICAM is constructed with nonhydrostatic equations (Tomita and Satoh, 2004). Furthermore, the model program is designed for an efficient parallel computation with Message Passing Interface (MPI) libraries (Tomita et al., 2008; Kodama et al., 2014). In fact, NICAM has been used for global nonhydrostatic high-resolution simulations with 14 km to 850 m grid resolutions (Miura et al., 2007; Miyamoto et al., 2013; Miyakawa et al., 2014). Nonetheless, in this study, we use a moderate resolution to reduce the high computational cost associated with the GHG inversion that requires repeated long-term simulations.

We set the horizontal resolution at "glevel-5" (Fig. 1). The "5" in glevel-5 denotes the number of division of the icosahedron. NICAM adopts the finite-volume method (Tomita and Satoh, 2004), whose control volume is a shaped pentagon at twelve vertices of the original icosahedron and hexagon at other grids (Fig. 1b). Those control volumes are constructed by connecting mass centers of the triangular elements that are produced by the recursive division of the icosahedron (Fig. 1a). The mean grid interval of glevel-5 is approximately 240 km. Although this horizontal resolution is much coarser than the high-resolutions that NICAM mainly targets, it is still comparable to the resolutions used in previous GHG inversion studies (e.g., Peylin et al., 2013; Le Quéré et al., 2016).

Because the dynamical core is constructed with the finite-volume method, NICAM achieves the consistency with continuity (CWC: Gross et al., 2002) for tracer transport (Satoh et al., 2008; Niwa et al., 2011b), which cannot be achieved in spectral AGCMs (Jöckel et al., 2001). Due to this CWC characteristic, tracer mass is perfectly conserved without any numerical mass fixer. Indeed, thanks to this property of CWC, atmospheric transport studies have been conducted using NICAM-TM with glevel-5. The model reproduces reasonably well the synoptic scale and vertical variations of radon (^{222}Rn) and the inter-hemispheric gradients of sulfur hexafluoride (SF_6) at the surface and in the upper troposphere (Niwa et al., 2011b, 2012).

The model configuration in this study is essentially the same as the one described in Niwa et al. (2012), except for the cumulus parameterization. The cumulus parameterization scheme is changed from Arakawa and Schubert (1974) to Chikira and Sugiyama (2010). The number of vertical model layers is 40, 12 layers of which exist below about 3 km. The top of the model domain is at about 45 km. The tracer advection process is calculated with the scheme of Miura (2007), and the vertical turbulent mixing is calculated with the MYNN (Mellor and Yamada, 1974; Nakanishi and Niino, 2004) Level 2 scheme (Noda et al., 2010). The model time step of glevel-5 is 20 min, both for the online and offline calculations. For the nudging used in the online calculation, we use the 6-hourly horizontal wind velocities of the Japan Meteorological Agency Climate Data Assimilation System (JCDAS) reanalysis data (Onogi et al., 2007).

2.2 Offline NICAM-TM

As is the case in the online model, the offline model integrates tracer mass ρq (ρ is air mass density and q is tracer mixing ratio) as

$$\frac{\partial \rho q}{\partial t} = \nabla \cdot (\rho \boldsymbol{v} q) + \frac{\partial}{\partial z}\left[\rho K_{\mathrm{v}} \left(\frac{\partial q}{\partial z}\right)\right] + f_{\mathrm{c}}(\rho, q_{\mathrm{w}}, T, M_{\mathrm{B}}, q), \quad (1)$$

where ∇ and $\boldsymbol{v}$ are the 3D divergence operator and wind vector, respectively, and K_{v} is the vertical diffusion coefficient. On the right hand side of the equation, the first and second terms represent the grid-scale tendency of advection and the sub-grid-scale tendency of vertical diffusion, respectively. The third term f_{c} denotes the sub-grid-scale tendency of cumulus convection, determined by ρ and the mixing ratios of water substances (q_{w}), temperature (T), and cumulus base mass flux (M_{B}).

Table 1 shows the archived meteorological parameters that drive the offline model. Integrative time resolutions of these parameters are thinned out (i.e., reduced) from the model time step interval of 20 min to several hours. In this study, we examine the sensitivity of the model results to changes in the time resolution of each of the driving meteorological transport variables (advection, vertical diffusion, and cumulus convection; Sect. 3.2).

In the archiving of the meteorological data, averaged values are saved for the air mass flux $\mathbf{V}$ ($= \rho \boldsymbol{v}$), while instantaneous values are saved for other meteorological parameters. The averaging of $\mathbf{V}$ is intended to preserve the CWC property. Originally, NICAM calculates the tracer advection using time-averaged air mass fluxes that are derived from air mass fluxes at a shorter time interval. The tracer advection is calculated with the Euler scheme, while momentums are

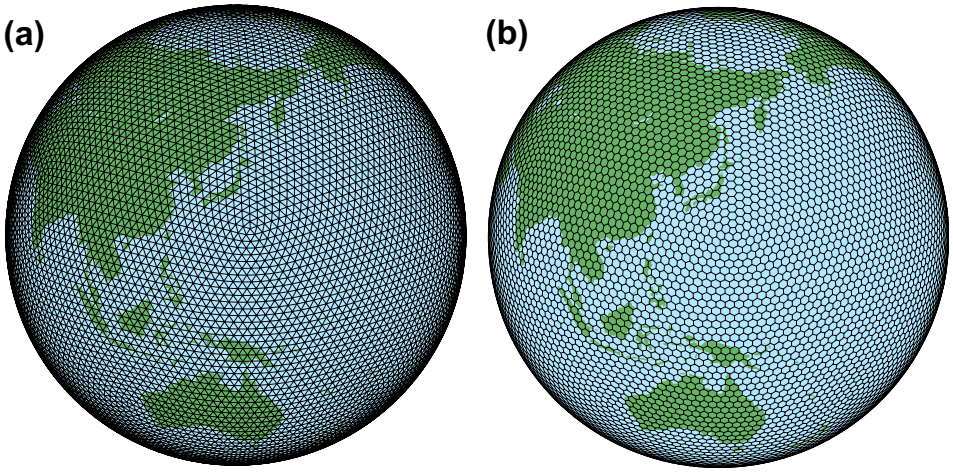

Figure 1. The grid distribution of NICAM glevel-5. Triangular elements produced by dividing an icosahedron five times **(a)** and control volumes constructed by connecting the mass centers of the triangular elements **(b)**.

Table 1. Meteorological parameters used for the offline forward and adjoint models.

Parameter	Symbol	Time type	Related process
Air mass density	ρ	Snapshot	Advection
Air mass flux	$\mathbf{V}$ $(=\rho\boldsymbol{v})$	Averaged	Advection
Vertical diffusion coefficient	K_v	Snapshot	Vertical diffusion
Water substances	q_w	Snapshot	Cumulus convection
Temperature	T	Snapshot	Cumulus convection
Cumulus base mass flux	M_B	Snapshot	Cumulus convection

calculated at a shorter time interval using the Runge–Kutta scheme. The time-averaged air mass flux retains the CWC property (Satoh et al., 2008; Niwa et al., 2011b). The offline model uses air mass fluxes that are further averaged for the thinning interval as

$$\overline{\mathbf{V}}^t = \frac{1}{N}\sum_{i=1}^{N}\mathbf{V}^{t+i\Delta\tau}, \tag{2}$$

where Δt is the thinning interval, $\Delta\tau$ is the model time step, and N is the integer defined as $N = \Delta t/\Delta\tau$. The offline calculation, whose time step is the same as that of the online, uses the above repeatedly during N steps from t to $t+\Delta t$ as

$$(\rho q)^{t+(i+1)\Delta\tau} = (\rho q)^{t+i\Delta\tau} + \Delta\tau\left(\nabla\cdot\overline{\mathbf{V}}^t q^{t+i\Delta\tau}\right). \tag{3}$$

In order to preserve CWC, ρ is simultaneously integrated with the same time-averaged air mass flux as

$$\rho^{t+(i+1)\Delta\tau} = \rho^{t+i\Delta\tau} + \Delta\tau\left(\nabla\cdot\overline{\mathbf{V}}^t\right) + \alpha, \tag{4}$$

where α is the modification term. If $\alpha = 0$, the Lagrangian conservation ($\mathrm{d}q/\mathrm{d}t = \partial q/\partial t + \boldsymbol{v}\cdot\nabla q = 0$) is achieved, which can easily be shown by substituting Eq. (4) to Eq. (3). In practice, α is nonzero and the Lagrangian conservation is not strictly satisfied due to evaporation and precipitation (note that ρ includes not only dry air but also water substances). This α is calculated as

$$\alpha = \frac{1}{N}\left(\rho^{t+\Delta t} - \rho^t - \Delta t\left(\nabla\cdot\overline{\mathbf{V}}^t\right)\right), \tag{5}$$

so that the integrated ρ with Eq. (4) after N steps coincides with $\rho^{t+\Delta t}$ that is provided from the online calculation. The other meteorological parameters (K_v, q_w, T and M_B) are linearly interpolated from the thinned interval steps to the model time steps.

2.3 Adjoint NICAM-TM

When $\mathbf{M}$ represents a forward model matrix and $\boldsymbol{a}$ and $\boldsymbol{b}$ are arbitrary vectors, an adjoint model matrix $\mathbf{M}^*$ satisfies $\langle\boldsymbol{a}, \mathbf{M}\boldsymbol{b}\rangle = \langle\mathbf{M}^*\boldsymbol{a}, \boldsymbol{b}\rangle$, where $\langle .,.\rangle$ is an inner product. In the usual case, the inner product is defined as $\langle\boldsymbol{a}, \boldsymbol{b}\rangle = \boldsymbol{a}^\mathrm{T}\boldsymbol{b}$; therefore, $\mathbf{M}^*$ is equivalent to $\mathbf{M}^\mathrm{T}$. In practice, $\boldsymbol{b}$ represents mixing ratio or surface flux and $\boldsymbol{a}$ is its adjoint variable. An adjoint model integrates adjoint variables backward in time to calculate sensitivities.

An adjoint model is constructed based on the above offline forward model. The adjoint model reads the archived meteorological data in the same way as the offline model, but in

reverse. Furthermore, similar to Eq. (4), ρ is simultaneously integrated with the reversed winds and $-\alpha$ in place of α.

For the vertical diffusion and cumulus convection processes, we use the discrete adjoint approach in which linear program codes are transposed. For the advection process, we employ both the discrete and continuous approaches. In the discrete adjoint approach, we give up the monotonicity. In NICAM, the tracer monotonicity is achieved by the use of the flux limiter of Thuburn (1996) (Miura, 2007; Niwa et al., 2011b). In fact, this flux limiter improves the model accuracy to some extent (Miura, 2007). All the transport calculations other than the flux limiter are linear. Therefore, we obtain a completely linear forward model by just switching off the flux limiter. From that linear forward model, we construct the adjoint model by transposing the linear codes. Because of the linearity, this adjoint model is expected to have the exact adjoint relationship with the forward model (with the flux limiter off), as proven in Sect. 3.4. The relationship is expressed as

$$(\mathbf{M}\boldsymbol{x})^{\mathrm{T}}\boldsymbol{y} = \boldsymbol{x}^{\mathrm{T}}\left(\mathbf{M}^{\mathrm{T}}\boldsymbol{y}\right), \tag{6}$$

where $\boldsymbol{x}$ and $\boldsymbol{y}$ represent the model input parameter vector and the observation vector, respectively. By giving up the monotonicity, however, the discrete adjoint produces negative (or oscillatory) sensitivities.

In the second approach, a continuous adjoint model is developed by discretizing the continuous adjoint equation (Sandu et al., 2005; Hakami et al., 2007; Gou and Sandu, 2011). In this approach, the flux limiter can be employed not only in the forward model, but also in the adjoint model, keeping the tracer concentrations or sensitivities positive (or non-oscillatory). However, due to the nonlinearity of the flux limiter, the adjoint relationship is no longer exact. The continuous adjoint equation of advection is written as

$$-\frac{\partial q^*}{\partial t} = \nabla\cdot\left(\boldsymbol{v}q^*\right), \tag{7}$$

where q^* is the adjoint variable for q. Equation (7) can be derived with the method of Lagrange multipliers and partial integrals from the advection part of Eq. (1) (a detailed derivation can be found in Sandu et al., 2005). Let $\widetilde{q}^* = q^*/\rho$, and we obtain

$$-\frac{\partial \rho\widetilde{q}^*}{\partial t} = \nabla\cdot\left(\rho\boldsymbol{v}\widetilde{q}^*\right). \tag{8}$$

By comparing Eq. (8) with Eq. (1), we find that we can reuse the divergence operator of the forward code by reversing the wind direction and integrating it backward in time. Thus, we can employ the nonlinear flux limiter to maintain the monotonicity of $\widetilde{q}^*$.

All the adjoint codes are manually written, achieving numerical efficiency of the model. Some studies use an automatic differentiation tool to readily create the adjoint model, but this carries the risk of making the model numerically inefficient. Furthermore, we retain the parallel computational ability of NICAM, allowing for significant savings in computational time.

2.4 CO_2 flux data

For the validation of the offline forward model, we simulate atmospheric CO_2 for the year 2010. For the surface boundary CO_2 flux input to the model, we use the inversion flux of Niwa et al. (2012) that is optimized for atmospheric CO_2 concentrations for 2006–2008. The inversion (posterior) flux consists of prior flux data sets and monthly flux adjustments derived from the observations. In this study, we replace the prior flux data sets with those for 2010 other than the climatological air–sea exchange data from Takahashi et al. (2009). We use the monthly data of fossil-fuel emission from the Carbon Dioxide Information Analysis Center (CDIAC) (Andres et al., 2013), of biomass burning emission from the Global Fire Emissions Database ver. 3.1 (van der Werf et al., 2010), and of terrestrial biosphere net ecosystem production (NEP) from the Carnegie–Ames–Stanford Approach (CASA) model (Randerson et al., 1997). To represent the diurnal variation of the terrestrial biosphere flux, we redistribute the monthly CASA NEP into 3-hourly fluxes using the same method as Olsen and Randerson (2004) using 2 m height air temperature and downward shortwave radiation data of JCDAS for 2010. Although the integrated surface CO_2 flux input to the model does not necessarily represent the actual flux variations in 2010, the overall resulting atmospheric CO_2 concentration field is consistent with the actual observed CO_2 concentrations, permitting an effective evaluation of the model transport performance. The initial concentration field is also constructed by running the model with the inversion flux for 2003–2009.

3 Results

3.1 Computational cost

All the simulations are performed on PRIMEHPC FX100 with MPI parallelization by 10 nodes (each node has 32 cores). For the 1-year-long sensitivity test simulation discussed below, the offline forward model requires only 7 min, while the online model requires about 70 min. Therefore, the offline model is 10 times faster computationally than the online model. The corresponding adjoint calculation also requires 7 min, therefore the 4D-Var calculation is demonstrated to be reasonably feasible. These computational costs are evaluated using the highest temporal resolution of the input meteorological data in the following sensitivity runs (A3V1C3, see below). However, we found that the computational costs are not significantly affected by the data thinning interval.

3.2 Evaluation of the data thinning error

As described in Sect. 2.2, the offline model can use a different data-thinning interval for each transport process. In order to determine an appropriate data-thinning interval, we perform five sensitivity runs (A6V6C6, A3V6C6, A3V6C3, A3V3C3, A3V1C3), changing the interval from 6 to 1 h, as shown in Table 2. In addition, we test A3V1C3 with the flux limiter in the advection scheme switched off (which is the counterpart of the discrete adjoint).

Figure 2 shows a zonal mean pressure–latitude cross-section of the root-mean-square deviation (RMSD) in CO_2 concentrations between the offline and online models. The RMSD value is calculated from hourly model output. The RMSD value represents the error induced only by the data thinning. Generally, the RMSD values are small even in the coarsest resolution case in which all the transport processes are calculated with 6-hourly data (A6V6C6). In most areas, the RMSDs are less than 1 ppm, indicating that the atmospheric transport is generally well simulated by the 6-hourly resolution. The relative error, which is defined as RMSD divided by the standard deviation of the concentration variation simulated by the online model, is 12.9 and 5.3 % on average at the surface and 300 hPa, respectively (Table 2).

A closer examination shows that the temporal resolution of each transport process affects the spatial distribution of RMSD. As shown in Fig. 2a and b, halving the interval of the advection data from A6V6C6 to A3V6C6 does not significantly reduce RMSDs, with the relative errors at the surface and 300 hPa decreasing slightly to 12.7 (from 12.9) and 4.8 (from 5.3) %, respectively. However, the RMSDs values are noticeably reduced in the mid- to upper troposphere when halving the interval of the cumulus convection data from A3V6C6 to A3V6C3, with the relative error in 300 hPa reduced to 3.3 %. This indicates a significant role of cumulus convection in CO_2 concentration variations in the mid- to upper troposphere. Furthermore, when increasing the temporal resolution of the vertical diffusion coefficient from A3V6C3 to A3V3C3, and to A3V1C3, we find greater RMSD reductions near the surface (Fig. 2d and e). The relative errors at the surface are reduced to 6.3 and 2.6 % for A3V3C3 and A3V1C3, respectively. This is attributable to the fact that vertical diffusion has a much higher temporal variability than the other transport processes, especially near the surface.

When the flux limiter is switched off in the A3V1C3 case, RMSDs are increased globally (Fig. 2f). The region where the RMSD has most pronouncedly increased is the stratosphere. This is probably because the flux limiter no longer suppresses the numerical oscillation near the top of the model domain, which is much larger than the CO_2 concentration variations in the stratosphere. However, in the troposphere, the numerical oscillations are not so large compared to the CO_2 concentration variations. Consequently, the relative error is 7.5 % at the surface, which is larger than A3V1C3 but less than the 6-hourly vertical diffusion cases (A6V6C6, A3V6C6, A3V6C3), and 9.0 % at 300 hPa, which is the highest number in all the sensitivity tests (Table 2).

Figure 3 shows the annual mean difference of CO_2 concentration at the surface between the offline and online models, for A6V6C6, A3V3C3, A3V1C3, and A3V1C3 without the flux limiter. In fact, these differences represent biases from the online calculation induced by the data thinning. Figure 3a shows that even the lowest temporal resolution of 6-hourly data input (A6V6C6) reproduces the CO_2 concentrations over the oceans well, where the bias is quite small (< 0.2 ppm). Meanwhile over the terrestrial areas, we see significantly larger biases. Specifically, they are more than 4 ppm over the tropical regions of the Amazon and Africa; these values are all negative due to systematically smaller nighttime accumulation, i.e., larger mixing, than the online model. Furthermore, since the results of A3V6C6 and A3V6C3 are very similar to that of A6V6C6, the resolution of the vertical diffusion coefficient data is a major factor contributing to the data-thinning error, particularly over the terrestrial biosphere in the summertime when strong diurnal variations exist. These biases are reduced but still larger than 1 ppm even when halving the temporal interval (A3V3C3; Fig. 3b). However, by increasing the temporal resolution of the vertical diffusion coefficient data to hourly, the biases become nearly indiscernible (A3V1C3; Fig. 3c). Since we still use the moderate resolution of a 3-hourly time step for the advection and cumulus convection processes, the necessary disk storage of A3V1C3 for 1 year is not extremely large (approximately 50 GB, after partially performing 2-byte data compression). Therefore, we set the A3V1C3 configuration to be the default for the glevel-5 simulations. When the flux limiter is switched off in A3V1C3, the bias increases slightly over the terrestrial areas but remains mostly less than 1 ppm (Fig. 3d). This bias is relatively small compared to the RMSD shown in Fig. 2f. Therefore, A3V1C3 without the flux limiter would be permissible only if the focus is on the concentration in the troposphere. This model configuration should be used when the model linearity is stringently required, such as in the use with the discrete adjoint.

3.3 Comparison with observations

In order to assess the magnitude of the offline model error, we compare the simulated CO_2 concentrations with the observed measurements at Minamitorishima, located in the western North Pacific (Wada et al., 2011), at Karasevoe, located in west Siberia (Sasakawa et al., 2010), and with the continuous aircraft CONTRAIL (Comprehensive Observation Network for Trace gases by Airliner: Machida et al., 2008) measurements obtained at 8–10 km altitude over Narita, Japan (each observation location is shown in Fig. 3a), representing marine background, continental, and upper-troposphere conditions, respectively.

Figure 4 shows the observed and simulated CO_2 concentrations at each site. Generally, the online model reproduces

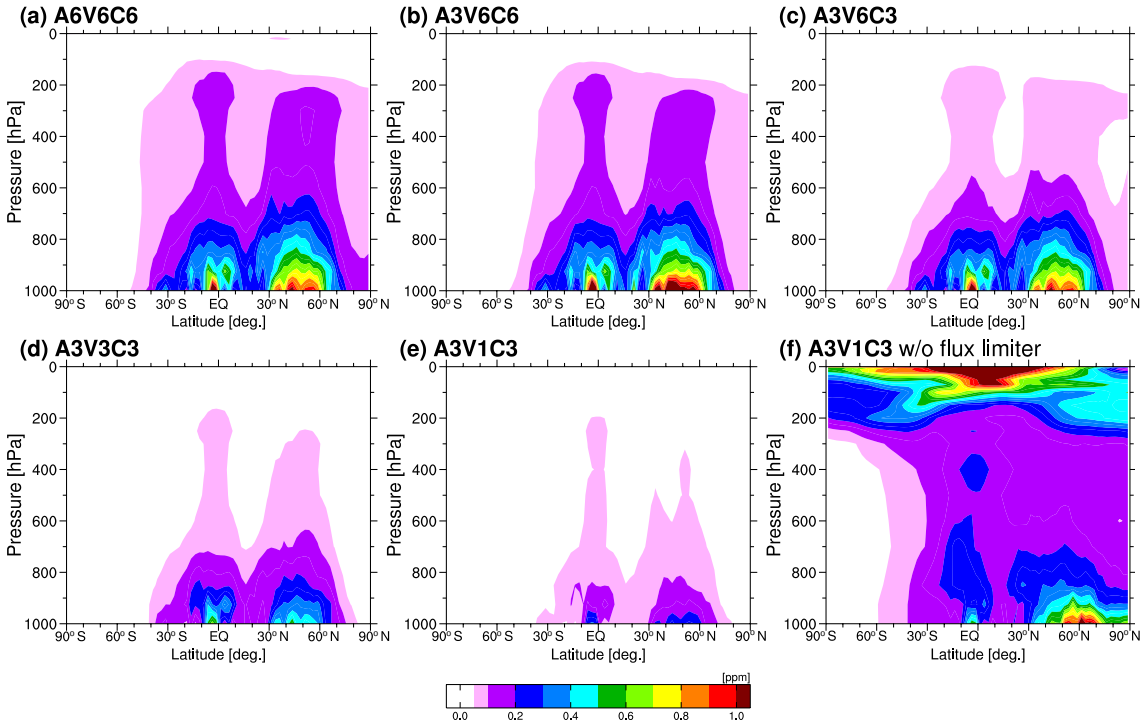

Figure 2. Zonal-mean latitude–pressure cross-section of annual root-mean-square deviation (RMSD) of CO_2 concentration simulated by the offline model against the online model. Time interval of the meteorological driver data is changed for each transport process as shown in Table 2 **(a–e)** and the same time resolutions are used as **(e)** but with the flux limiter switched off **(f)**.

Table 2. Temporal intervals for advection, vertical diffusion, and cumulus convection processes in each sensitivity test and relative errors globally averaged at the surface and 300 hPa. The relative error is calculated at each model grid by dividing RMSD by the standard deviation of the CO_2 concentration variation simulated by the online model for 2010.

Notation	Temporal interval (h)			Relative error (%)	
	Advection	Vertical diffusion	Cumulus convection	Surface	300 hPa
A6V6C6	6	6	6	12.9	5.3
A3V6C6	3	6	6	12.7	4.8
A3V6C3	3	6	3	12.6	3.3
A3V3C3	3	3	3	6.3	2.2
A3V1C3	3	1	3	2.6	2.0
A3V1C3 w/o flux limiter	3	1	3	7.5	9.0

the observed CO_2 concentration variations relatively well, partly due to the inversion flux we use. In the inversion, we used the Minamitorishima and CONTRAIL data to constrain the terrestrial biosphere and ocean fluxes (Niwa et al., 2012). However, the high reproducibility of the synoptic variations indicates reasonable transport performance of NICAM-TM, given the fact that we used monthly mean observations in the inversion. Table 3 shows correlation coefficients of the synoptic variations between the simulated and observed concentrations at the three sites, all of which are found to be statistically significant. Here, the synoptic variations are defined by residual CO_2 concentrations from a smoothed curve represented by a linear trend and three harmonics, similarly to Patra et al. (2008).

At Minamitorishima and over Narita, the RMSD values between the observation and the model are quite small; 0.92 and 1.36 ppm, respectively. Compared to those RMSDs, the RMSD between the offline and online models is negligibly small, even for the lowest resolution of A6V6C6 (Fig. 4a and c). Furthermore, changes in the correlation coefficients of the synoptic variations are also quite small (Table 3). These negligible influences of the data thinning are accentuated by comparing with an additional online simulation in which different wind data from the Japanese 55-year Reanalysis (JRA-

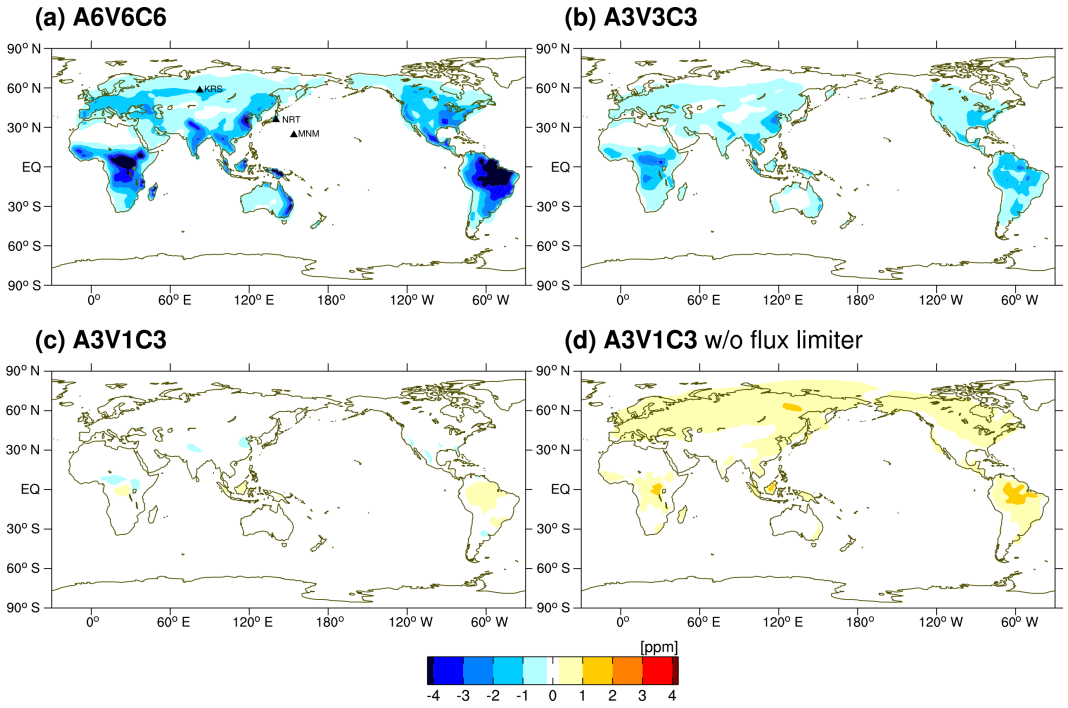

Figure 3. Annual mean difference of CO_2 concentration at the surface model layer between the offline and online models (offline minus online) for each sensitivity test: A6V6C6 **(a)**, A3V3C3 **(b)**, A3V1C3 **(c)**, and A3V1C3 without the flux limiter **(d)**. White colored areas signify absolute values less than 0.2 ppm. The geographical locations of Minamitorishima (MNM), Karasevoe (KRS), and Narita (NRT) are also indicated in **(a)**.

Table 3. Temporal correlation coefficients of simulated residual CO_2 concentrations (see the text for details) with the observations at Minamitorishima, Karasevoe, and 8–10 km altitude over Narita for the online and offline (A6V6C6 and A3V1C3) simulations. The results of A3V1C3 without the flux limiter and the online model nudged by JRA-55 are also shown.

Site	Online	A6V6C6	A3V1C3	A3V1C3 w/o flux limiter	Online nudged by JRA-55
Minamitorishima	0.577	0.572	0.575	0.573	0.587
Karasevoe	0.610	0.579	0.613	0.607	0.609
Narita 8–10 km	0.323	0.318	0.324	0.311	0.302

55: Kobayashi et al., 2015; Harada et al., 2016), instead of JCDAS, are used for the nudging. The RMSD values between the two online models (JCDAS versus JRA-55) are 0.22 and 0.40 ppm, respectively, for Minamitorishima and over Narita, which are larger than the RMSDs between the online and offline models. Also, the correlation coefficient change from JCDAS to JRA-55 is larger than the changes from the online to the offline (Table 3). In fact, these correlation coefficients would change more distinctly with a different model, given the fact that Patra et al. (2008) showed a large range of the correlation coefficients (∼ 0.4–0.7) for Minamitorishima among multiple models.

However, for A6V6C6 at the continental site, Karasevoe, we found a significant influence of the data thinning. Here, the RMSD between the observation and the online model is 5.72 ppm, probably due to the fact that the observation is independent of the inversion and consequently the flux data have a large error for this area. Comparably, the meteorological resolution of A6V6C6 results in an RMSD value of 2.93 ppm. As shown in Fig. 4b, the offline model produces lower CO_2 values compared to those produced by the online model during the summer. As stated earlier, this is likely due to the systematically smaller nighttime accumulation and is the cause of the negative bias against the online model shown in Fig. 3a. This lower CO_2 of A6V6C6 does not necessarily cancel out the positive deviations of the online model from the observation (Fig. 4b) and hence is not closer to the observation than the online model. In fact, the correlation coefficient of the synoptic variations diminishes from the online model to A6V6C6 (from 0.610 to 0.579), whose magnitude is relatively large compared to the other changes (Table 3). By increasing the temporal resolution of the vertical

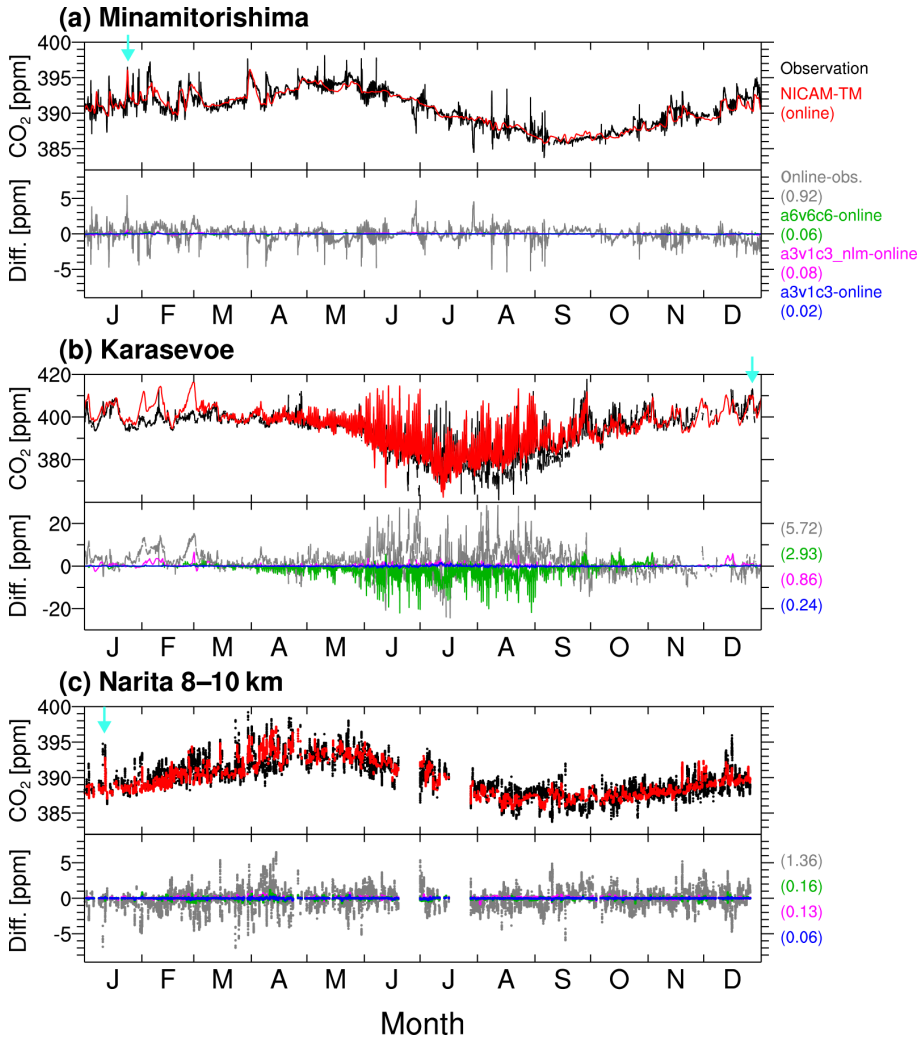

Figure 4. Time series of CO_2 concentration for 2010 at Minamitorishima **(a)**, Karasevoe **(b)**, and 8–10 km altitude over Narita **(c)**. Each upper panel shows the time series observed (black) and simulated by the online model (red). Each lower panel shows differences of CO_2 concentrations between the online model and the observation (gray), and between the offline model (green for A6V6C6, magenta for A3V1C3, and blue for A3V1C3 without the flux limiter) and the online model. The number in the parenthesis gives the RMSD value for each sensitivity case. Note that only tropospheric data (determined by the dynamical tropopause; Sawa et al., 2008) are used for the comparison over Narita.

diffusion coefficient to hourly (A3V1C3), we obtain a sufficiently small RMSD value of 0.24 ppm compared to the online model.

Without the flux limiter, the RMSDs are modestly small (at most 0.86 ppm for Karasevoe) and the difference does not have any distinct positive or negative tendency (Fig. 4). Meanwhile, the correlation coefficients are reduced by switching off the flux limiter coherently at the three sites (Table 3). Although they are all minute changes, they suggest that the flux limiter has improved the model accuracy.

3.4 Validation of the adjoint model

We now validate the exactitude of the adjoint model using the reciprocity property with its corresponding forward models. A detailed description of the reciprocity property can be found in the literature (Hourdin and Talagrand, 2006; Hourdin et al., 2006; Haines et al., 2014; Wilson et al., 2014). In Eq. (6), if $\boldsymbol{x}$ and $\boldsymbol{y}$ are the basis unit vectors having 1 for ith and jth elements, respectively, and 0 for all the others (i.e., $\boldsymbol{x} = (0\cdots0,1,0\cdots0)^{\mathrm{T}}$ and $\boldsymbol{y} = (0\cdots0,1,0\cdots0)^{\mathrm{T}}$), a value sampled at j, which is simulated from $\boldsymbol{x}$ with the forward model ($(\mathbf{M}\boldsymbol{x})^{\mathrm{T}}\boldsymbol{y} = (\mathbf{M}\boldsymbol{x})_j = M_{j,i}$), should coincide with the value simulated from $\boldsymbol{y}$ with the adjoint model and subsequently sampled at i ($\boldsymbol{x}^{\mathrm{T}}(\mathbf{M}^{\mathrm{T}}\boldsymbol{y}) = (\mathbf{M}^{\mathrm{T}}\boldsymbol{y})_i = M_{j,i}$). Checking this reciprocity, we can verify the exactitude of the adjoint code. To evaluate the reciprocity for both the discrete and continuous adjoint models, we use the forward model without and with the flux limiter, respectively. The former forward/adjoint model set is linear but does not ensure mono-

tonicity, while the latter set is nonlinear but ensures monotonicity. Both in the forward and adjoint model simulations, we use the configuration of A3V1C3 for the meteorological input.

For a case study, we examine an Asian outflow event, which is a typical transport phenomenon in East Asia during the winter–spring season (e.g., Sawa et al., 2007). We prescribe a surface flux at the model grid (X) located on the coast of East Asia representing the basis unit vector $\boldsymbol{x}$ (its location is denoted by the open cyan circle in Fig. 5b). Meanwhile, we prepare 160 observational basis unit vectors ($\boldsymbol{y}$), whose sampling points are regularly located at 3 km altitude over an area enclosed by 14–32° N and 111–159° E (denoted by cyan dots in Fig. 5a). The simulation period lasts for 7 days, starting on 1 January 2010. The flux is time invariant, i.e., the vector $\boldsymbol{x}$ is a function of space only. Figure 5a shows the concentration field at the end of the period, as simulated by the forward model with the flux limiter. In addition, Fig. 5b shows the sensitivities of the observation Y that is located at the eastern edge of the range (denoted by the cyan triangle in Fig. 5a) against the surface fluxes (i.e., footprint). This sensitivity is calculated by the continuous adjoint. We find that, using the discrete adjoint, the calculated footprint pattern is quite similar to that shown in Fig. 5b. This is not surprising since the forward simulation without the flux limiter does not introduce substantial errors in the troposphere, as previously shown. As the concentration field shown Fig. 5a is simulated from the unit flux, it also represents the degree of spatial sensitivity between the flux and the observation. According to Eq. (6), the concentration value sampled at the observation point Y should coincide with the footprint value located at the flux point X. By performing adjoint simulations for the remaining 159 observation points, we can evaluate the overall reciprocity of the adjoint model.

Figure 6 shows a scatter diagram of the 160 pairs of forward concentration values at the observation points with their corresponding adjoint footprint values at the flux point X. It can be seen in the figure that the footprint values simulated by the discrete adjoint completely correspond to the forward concentration values within computer machine accuracy. This demonstrates that the discrete adjoint has the exact reciprocity against the forward model without the flux limiter. Conversely, the continuous adjoint does not have the exact reciprocity but it is reasonably approximated. Figure 6 also demonstrates that the continuous adjoint successfully avoids negative sensitivities because of the flux limiter, while the discrete adjoint calculation does produce negative sensitivities.

3.5 Adjoint trajectory analysis

Finally, we apply the adjoint sensitivities to a transport trajectory analysis. Generally, the adjoint model provides sensitivities of a specified scalar value with respect to concentrations and surface fluxes (Appendix A). When the scalar value is set to an observed concentration, the cost functional is defined as

$$J = \int_{t}^{t_\mathrm{o}} \int_{\Omega} g(q) d\Omega \mathrm{d}t', \tag{9}$$

$$g(q) = q(x,t')\delta(x - x_\mathrm{o})\delta(t' - t_\mathrm{o}), \tag{10}$$

where δ is the delta function and x_o and t_o represent the observed location and time, respectively. Therefore, the value of the cost functional corresponds to the observed concentration $q(x_\mathrm{o}, t_\mathrm{o})$. According to Appendix A, the change of the cost functional is given by

$$\Delta J = \Delta q(x_\mathrm{o}, t_\mathrm{o}) = \int_{t}^{t_\mathrm{o}} \int_{\Omega} \left(\mathcal{F}^* q^*(x,t')\right) \Delta s(x,t') \mathrm{d}\omega \mathrm{d}t' + \int_{\Omega} q^*(x,t) \Delta q(x,t) \mathrm{d}\omega, \tag{11}$$

where $\mathcal{F}^*$ represents the adjoint of the transferring operator from flux to concentration, and Δs denotes the flux perturbation. $\mathcal{F}^* q^*$ and q^* denote the sensitivities of the observed concentration with respect to the surface flux and concentration, respectively. If considered processes are all linear (which is the case in this study since we consider only atmospheric transport), we can omit Δ. Then, the first and second terms represent respectively the actual contributions of the surface flux from t to t_o and the concentration at t to the observed concentration. For our analysis, we investigate the spatial structures of these sensitivity quantities normalized by $q(x_\mathrm{o}, t_\mathrm{o})$, i.e., $\int_t^{t_\mathrm{o}} \left(\mathcal{F}^* q^*(x,t')\right) s(x,t') \mathrm{d}t' / q(x_\mathrm{o}, t_\mathrm{o})$ and $q^*(x,t) q(x,t) / q(x_\mathrm{o}, t_\mathrm{o})$. These quantities derived by the adjoint model have been utilized in previous studies for diagnosing trace gas transport in the atmosphere (Vukićević and Hess, 2000; Hess and Vukicevic, 2003) and a pathway of a water mass in the ocean (Fujii et al., 2013).

Using such adjoint-derived quantities, we analyze three high CO_2 concentration events, observed at Minamitorishima on 24 January, at Karasevoe on 27 December, and at 8 km over Narita on 12 January 2010 (denoted by the cyan arrows in Fig. 4). These high-concentration events are chosen because NICAM-TM captures this event well (see Fig. 4). Figure 7 shows the normalized flux contribution and "adjoint trajectory volumes" (Hess and Vukicevic, 2003) against each event. The adjoint trajectory volume is derived by averaging $q^*(x,t) q(x,t) / q(x_\mathrm{o}, t_\mathrm{o})$ for each day prior to the observation period. Overlaying the averaged $q^*(x,t) q(x,t) / q(x_\mathrm{o}, t_\mathrm{o})$ shows the pathway of the air mass that caused each of the high CO_2 events at the observation location and time. This analysis approach resembles the one taken by Hess and Vukicevic (2003). The forward simulation that calculates $q(x,t)$ and the adjoint simulation that calculates $q^*(x,t)$ and $\mathcal{F}^* q^*(x,t)$ are performed for 1 week prior to each observation period. Here, we show the results calculated by the continuous adjoint model, taking the advantage

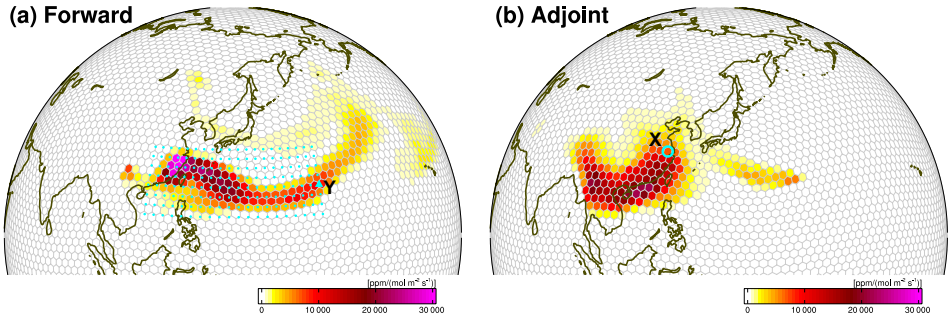

Figure 5. The concentration field at 3 km altitude on 00:00 UTC 8 January 2010 simulated by the forward model (with the flux limiter) from the basis unit flux X **(a)** and the sensitivities of the observation Y against the surface fluxes (footprint) simulated by the continuous adjoint model **(b)**. The observation points, from which the adjoint sensitivities are calculated, are denoted as cyan dots and the location of observation Y is indicated by the cyan triangle **(a)**. The location of the basis unit flux X is indicated by the open cyan circle **(b)**.

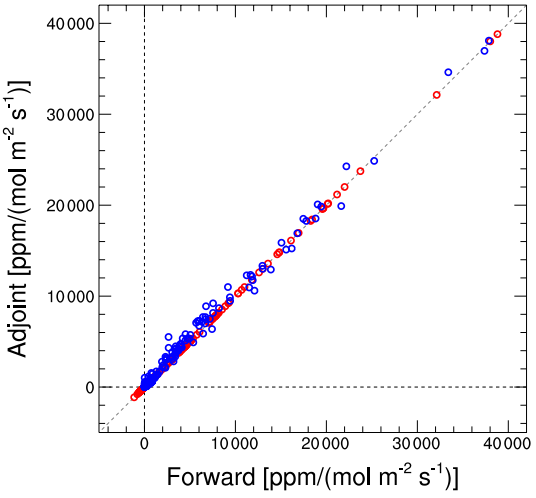

Figure 6. The scatter diagram showing 160 concentration values simulated by the forward model at the observation points versus their corresponding adjoint footprint values at the flux point X. The open red circles denote values from the linear model setup (the forward model without the flux limiter and the discrete adjoint model), while the open blue circles denote values from the nonlinear model setup (the forward model with the flux limiter and the continuous adjoint model).

of its monotonicity property. However, the discrete adjoint model produces similar sensitivity features (not shown).

Interestingly, the analysis indicates that three high concentration events were produced by three distinctly different transport phenomena. The flux contribution shows that the event observed at Minamitorishima originated from the Korean Peninsula and eastern China (Fig. 7a). Furthermore, the sharp adjoint trajectory volume indicates that the transport of the high CO_2 plume was characterized by slow diffusion. For the event observed at Karasevoe, the analysis indicates that the air mass that produced the high CO_2 concentration was advected from the west, but fluxes in the vicinity of the observation site also contributed to the observed concentration (Fig. 7b). This local flux contribution is a result of a very shallow mixed layer, as indicated by the vertical structure of the trajectory volume that is concentrated below 1 km. Figure 7c shows that the high concentration event observed over Narita originated from southeast China. The adjoint trajectory volume indicates that the horizontal transport of the air mass from China to Japan was fast (taking only about 2 days) compared to the other cases because of the strong westerlies in the free troposphere. Before this fast eastward transport, the analysis also indicates the possibility of an air mass propagation westward along the slope of the topography. Therefore, this result suggests that the topographical uplifting may play a significant role in high CO_2 concentration events frequently observed over Narita (Shirai et al., 2012).

4 Conclusions

We have developed forward and adjoint models based on NICAM-TM, as part of the 4D-Var system for atmospheric GHGs inversions. Both of these models are offline. Therefore, the models are computationally efficient enough to make the 4D-Var iterative calculation feasible. The computational cost of the offline forward model is about 10 times less than that of the corresponding online model calculation, irrespective of the temporal resolution of the meteorological data input. Furthermore, the adjoint model computational cost is nearly the same as that of the forward model.

The archived meteorological data used in the forward and adjoint models were prepared by the online AGCM calculation of NICAM in advance. In this study, we have developed the variable temporal resolution capabilities for individual meteorological transport data to minimize the offline model errors due to the data thinning. Through sensitivity tests using CO_2 as a tracer, we have determined that the temporal resolution of the vertical diffusion coefficient should be high; otherwise, a significantly large systematic bias is introduced near the surface due to the smaller CO_2 accumulation during the nighttime. For the spatial resolution used in this

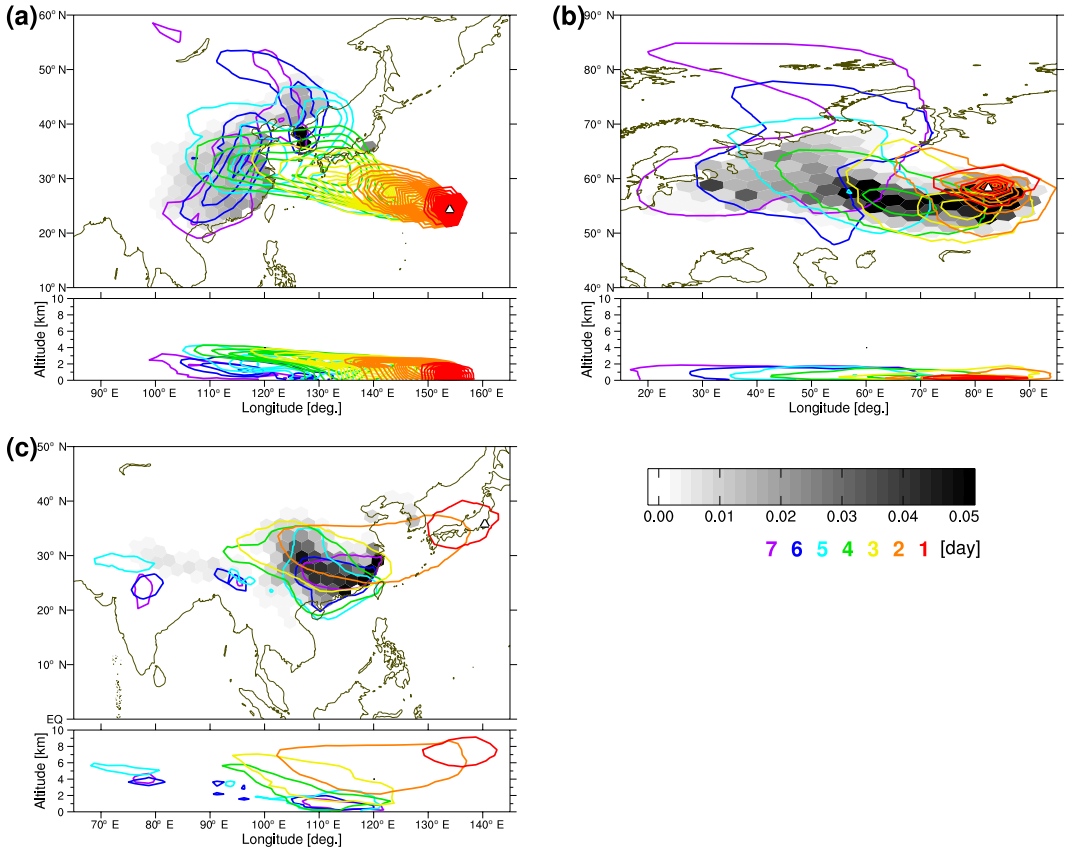

Figure 7. The normalized flux contributions (gray shades) and the adjoint trajectory volumes (color contours) are shown for the high CO_2 concentration events observed at Minamitorishima on 24 January **(a)**, at Karasevoe on 27 December **(b)**, and at 8 km over Narita on 12 January 2010 **(c)**, which are denoted by the cyan arrows in Fig. 4. See the text for the definitions of the flux contribution and the adjoint trajectory volume. The upper and lower panels present the horizontal and vertical structures of the adjoint trajectory volume, whose maximum values are projected onto the horizontal and vertical planes, respectively. The adjoint trajectory volumes are drawn with contours starting from a minimum value 0.02 at an interval of 0.6. The color of the contour represents how many days prior to the observation time to which the adjoint trajectory volume is associated.

study (the horizontal grid interval is approximately 240 km), the use of a 1 h interval for the vertical diffusion coefficient and 3 h interval for the other meteorological fields (A3V1C3) is enough to simulate CO_2 concentrations that are reasonably consistent with the online calculation. By comparing these with observations, we have found that the error from the data thinning in A3V1C3 is negligible compared with the intrinsic model performance. In a case without using the flux limiter, we have found significant errors in the stratosphere, while the errors in the troposphere were smaller and tolerable. Therefore, simulations without the flux limiter can be carried out in studies focused only on the troposphere.

For the adjoint model, we have explored the relative impact of using discrete adjoint or continuous adjoint on the advective transport process. Using an Asian outflow case, we have demonstrated the perfect adjoint relationship of the discrete adjoint with its corresponding forward model in which the flux limiter is turned off. In the same analysis, the continuous adjoint has also shown reasonable adjoint exactitude against the forward model with the flux limiter turned on. Furthermore, we have found that the adjoint model can be used in attribution studies in which surface flux contributions are diagnosed as a function of air mass pathway when interpreting observed high CO_2 concentration events.

Based on the results of this study, we have developed a new 4D-Var system for performing CO_2 inversions. Application of the 4D-Var system and its results are described in the accompanying paper by Niwa et al. (2016). In the accompanying paper, the A3V1C3 configuration is used to judge which of the adjoint calculation methods, discrete or continuous, is better suited for global inversion studies.

Icosahedral grid models such as NICAM are a new model type and are becoming popular in dynamical meteorology research fields as remarkable innovations in supercomputers are made. However, there are still only a few studies of its applications in atmospheric chemistry and inversion/assimilation calculations (e.g., Elbern et al., 2010). One prominent feature of the NICAM-TM 4D-Var system is the

perfect mass conservation, as described in Sect 2.1. Another advantage of the system is its computational efficiency when applied to linear GHG inversion problems. If we limit the analysis period to a short time, a global high-resolution inversion would be feasible as long as sufficient data storage capacity is available. Furthermore, regional high-resolution inversions would also be possible with the grid stretching technique (Tomita, 2008; Goto et al., 2015). It is expected that the system developed in this study and in the accompanying paper can exploit new observations and open up new avenues for GHG inversions.

Code availability. Development of NICAM-TM is being continued by the authors. The source codes of NICAM-TM are available for those who are interested. The source codes of NICAM-TM are included in the package of the parent model NICAM, which can be obtained upon request under the general terms and conditions (http://nicam.jp/hiki/?Research+Collaborations).

Appendix A: Adjoint sensitivity

Here we explain the theory of the adjoint sensitivity following the description of Vukićević and Hess (2000). The tracer transport equation can be written in the following compact form of

$$\mathcal{L}q = \mathcal{F}s, \tag{A1}$$

where $\mathcal{L}$ is the transport operator,

$$\mathcal{L} \equiv \frac{\partial}{\partial t} + \mathcal{A} + \mathcal{V} + \mathcal{C}. \tag{A2}$$

The operator $\mathcal{F}$ is transferring surface flux s to concentration, and the operators for advection, vertical diffusion, and cumulus convection are represented as $\mathcal{A}$, $\mathcal{V}$, and $\mathcal{C}$, respectively. Then, the adjoint operator $\mathcal{L}^*$ is defined as

$$\mathcal{L}^* \equiv -\frac{\partial}{\partial t} + \left(\mathcal{A}^* + \mathcal{V}^* + \mathcal{C}^*\right), \tag{A3}$$

where $\mathcal{A}^*$, $\mathcal{V}^*$, and $\mathcal{C}^*$ are the adjoint operators for $\mathcal{A}$, $\mathcal{V}$, and $\mathcal{C}$.

We characterize the solution of the tracer transport Eq. (A1) by the cost functional J as

$$J = \int_{t_1}^{t_2} \int_{\Omega} g(q) \mathrm{d}\omega \mathrm{d}t, \tag{A4}$$

where $[t_1, t_2]$ is the time interval examined, Ω is the spatial domain, $\mathrm{d}\omega$ is the area differential, and $g(q)$ is the diagnostic operator of q. Then the change from the perturbation of q is described as

$$\Delta J = \int_{t_1}^{t_2} \int_{\Omega} \frac{\partial g}{\partial q} \Delta q \ \mathrm{d}\omega \mathrm{d}t. \tag{A5}$$

The adjoint operator $\mathcal{L}^*$ defines an adjoint equation for the adjoint variable q^* as

$$\mathcal{L}^* q^* = \frac{\partial g}{\partial q}. \tag{A6}$$

Multiplying Eq. (A6) by Δq, and integrating over time and over the spatial domain, we obtain

$$\Delta J = \int_{t_1}^{t_2} \int_{\Omega} \left(\mathcal{L}^* q^*\right) \Delta q \ \mathrm{d}\omega \mathrm{d}t. \tag{A7}$$

By integration by parts, Eq. (A7) transforms into

$$\Delta J = \int_{t_1}^{t_2} \int_{\Omega} q^* \left(\mathcal{L}\Delta q\right) \mathrm{d}\omega \mathrm{d}t - \int_{\Omega} \left[q^* \Delta q\right]_{t_1}^{t_2} \mathrm{d}\omega - \int_{t_1}^{t_2} \left[q^* \Delta q\right]_{O(\omega)} \mathrm{d}t, \tag{A8}$$

where $O(\omega)$ denotes the boundary of the integration domain. Using Eq. (A1) and the adjoint operator $\mathcal{F}^*$ for $\mathcal{F}$, and specifying $q^* = 0$ at $t = t_2$ and $O(\omega)$ (no inflow/outflow of q^* at the boundary), we finally obtain

$$\Delta J = \int_{t_1}^{t_2} \int_{\Omega} \left(\mathcal{F}^* q^*(x,t)\right) \Delta s(x,t) \mathrm{d}\omega \mathrm{d}t - \int_{\Omega} q^*(x,t_1) \Delta q(x,t_1) \mathrm{d}\omega. \tag{A9}$$

In Eq. (A9), $\mathcal{F}^* q^*(x,t)$ and $q^*(x,t_1)$ represent the sensitivities of ΔJ against the flux change ($\Delta s(x,t)$) and the change of the concentration at t_1 ($\Delta q(x,t_1)$), which are generally called adjoint sensitivities. If the cost functional J represents an observed quantity, then $\int_{t_1}^{t_2} \mathcal{F}^* q^*(x,t) \mathrm{d}t$ expresses its footprint as shown in Fig. 5b.

Competing interests. The authors declare that they have no conflict of interest.

Acknowledgements. Comments from Maarten Krol and Arne Babenhauserheide helped to improve the manuscript. They were greatly appreciated. We also thank Kaz Higuchi of York University, Canada, for his fruitful comments on the manuscript. The Minamitorishima CO_2 observational data were downloaded from the World Data Centre for Greenhouse Gases (WDCGG). We would like to acknowledge the staff of Japan Meteorological Agency for providing the data via the WDCGG site. This study is supported mainly by the Environment Research and Technology Development Fund (2-1401) of the Ministry of the Environment, Japan. This study is also supported partly by the cooperative research for climate system of Atmosphere and Ocean Research Institute, the University of Tokyo, and by "advancement of meteorological and global environmental predictions utilizing observational Big Data" of the social and scientific priority issues (Theme 4) to be tackled by using Post-K computer of the FLAGSHIP2020 Project. The calculations of this study were performed on the supercomputer system, FUJITSU PRIMEHPC FX100, of Meteorological Research Institute.

Edited by: V. Grewe
Reviewed by: M. Krol and A. Babenhauserheide

References

Andres, R. J., Boden, T., and Marland, G.: Monthly Fossil-Fuel CO_2 Emissions: Mass of Emissions Gridded by One Degree Latitude by One Degree Longitude, Carbon Dioxide Information Analysis Center, Oak Ridge National Laboratory, U.S. Department of Energy, Oak Ridge, Tenn., USA, doi:10.3334/CDIAC/ffe.MonthlyMass.2013, 2013.

Arakawa, A. and Schubert, W. H.: Interaction of a cumulus cloud ensemble with the large-scale environment, Part I, J. Atmos. Sci., 31, 674–701, doi:10.1175/1520-0469(1974)031<0674:IOACCE>2.0.CO;2, 1974.

Baker, D. F., Doney, S. C., and Schimel, D. S.: Variational data assimilation for atmospheric CO_2, Tellus B, 58, 359–365, doi:10.1111/j.1600-0889.2006.00218.x, 2006.

Basu, S., Guerlet, S., Butz, A., Houweling, S., Hasekamp, O., Aben, I., Krummel, P., Steele, P., Langenfelds, R., Torn, M., Biraud, S., Stephens, B., Andrews, A., and Worthy, D.: Global CO_2 fluxes estimated from GOSAT retrievals of total column CO_2, Atmos. Chem. Phys., 13, 8695–8717, doi:10.5194/acp-13-8695-2013, 2013.

Bregman, B., Segers, A., Krol, M., Meijer, E., and van Velthoven, P.: On the use of mass-conserving wind fields in chemistry-transport models, Atmos. Chem. Phys., 3, 447–457, doi:10.5194/acp-3-447-2003, 2003.

Chevallier, F., Fisher, M., Peylin, P., Serrar, S., Bousquet, P., Bréon, F.-M., Chédin, A., and Ciais, P.: Inferring CO_2 sources and sinks from satellite observations: Method and application to TOVS data, J. Geophys. Res., 110, doi:10.1029/2005JD006390, 2005.

Chevallier, F., Ciais, P., Conway, T. J., Aalto, T., Anderson, B. E., Bousquet, P., Brunke, E. G., Ciattaglia, L., Esaki, Y., Fröhlich, M., Gomez, A., Gomez-Pelaez, A. J., Haszpra, L., Krummel, P. B., Langenfelds, R. L., Leuenberger, M., Machida, T., Maignan, F., Matsueda, H., Morguí, J. A., Mukai, H., Nakazawa, T., Peylin, P., Ramonet, M., Rivier, L., Sawa, Y., Schmidt, M., Steele, L. P., Vay, S. A., Vermeulen, A. T., Wofsy, S., and Worthy, D.: CO_2 surface fluxes at grid point scale estimated from a global 21 year reanalysis of atmospheric measurements, J. Geophys. Res., 115, doi:10.1029/2010JD013887, 2010.

Chikira, M. and Sugiyama, M.: A Cumulus Parameterization with State-Dependent Entrainment Rate. Part I: Description and Sensitivity to Temperature and Humidity Profiles, J. Atmos. Sci., 67, 2171–2193, doi:10.1175/2010JAS3316.1, 2010.

Elbern, H., Schwinger, J., and Botchorishvili, R.: Chemical state estimation for the middle atmosphere by four-dimensional variational data assimilation: System configuration, J. Geophys. Res., 115, doi:10.1029/2009JD011953, 2010.

Errico, R.: What Is an Adjoint Model?, B. Am. Meteorol. Soc., 78, 2577–2591, doi:10.1175/1520-0477(1997)078<2577:WIAAM>2.0.CO;2, 1997.

Fujii, Y., Nakano, T., Usui, N., Matsumoto, S., Tsujino, H., and Kamachi, M.: Pathways of the North Pacific Intermediate Water identified through the tangent linear and adjoint models of an ocean general circulation model, J. Geophys. Res., 118, 2035–2051, doi:10.1002/jgrc.20094, 2013.

Godunov, S.: A difference scheme for numerical computation of discontinuous solutions of equations in fluid dynamics, Matematicheskii Sbornik, 47, 271–306, 1959.

Goto, D., Dai, T., Satoh, M., Tomita, H., Uchida, J., Misawa, S., Inoue, T., Tsuruta, H., Ueda, K., Ng, C. F. S., Takami, A., Sugimoto, N., Shimizu, A., Ohara, T., and Nakajima, T.: Application of a global nonhydrostatic model with a stretched-grid system to regional aerosol simulations around Japan, Geosci. Model Dev., 8, 235–259, doi:10.5194/gmd-8-235-2015, 2015.

Gou, T. and Sandu, A.: Continuous versus discrete advection adjoints in chemical data assimilation with CMAQ, Atmos. Environ., 45, 4868–4881, doi:10.1016/j.atmosenv.2011.06.015, 2011.

Gross, E. S., Bonaventura, L., and Rosatti, G.: Consistency with continuity in conservative advection schemes for free-surface models, Int. J. Numer. Meth. Fl., 38, 307–327, 2002.

Haines, P. E., Esler, J. G., and Carver, G. D.: Technical Note: Adjoint formulation of the TOMCAT atmospheric transport scheme in the Eulerian backtracking framework (RETRO-TOM), Atmos. Chem. Phys., 14, 5477–5493, doi:10.5194/acp-14-5477-2014, 2014.

Hakami, A., Henze, D., Seinfeld, J., Singh, K., Sandu, A., Kim, S., Byun, D., and Li, Q.: The adjoint of CMAQ, Environ. Sci. Technol., 41, 7807–7817, doi:10.1021/es070944p, 2007.

Harada, Y., Kamahori, H., Kobayashi, C., Endo, H., Kobayashi, S., Ota, Y., Onoda, H., Onogi, K., Miyaoka, K., and Takahashi, K.: The JRA-55 Reanalysis: Representation of Atmospheric Circulation and Climate Variability, J. Meteorol. Soc. Jpn., 94, 269–302, doi:10.2151/jmsj.2016-015, 2016.

Heimann, M.: The Global Atmospheric Tracer Model TM2, Tech. Rep. 10, Max-Planck-Institut für Biogeochemie, Hamburg, Germany, 1995.

Heimann, M. and Keeling, C.: A three-dimensional model of atmospheric CO_2 transport based on obaserved winds: 2: Model description and simulated tracer experiments, Geophys. Monog. Series, 55, 237–275, 1989.

Hess, P. G. and Vukicevic, T.: Intercontinental transport, chemical transformations, and baroclinic systems, J. Geophys. Res., 208, doi:10.1029/2002JD002798, 2003.

Hourdin, F. and Talagrand, O.: Eulerian backtracking of atmospheric tracers. I: Adjoint derivation and parametrization of subgrid-scale transport, Q. J. Roy. Meteor. Soc., 132, 567–583, doi:10.1256/qj.03.198.A, 2006.

Hourdin, F., Talagrand, O., and Idelkadi, A.: Eulerian backtracking of atmospheric tracers. II: Numerical aspects, Q. J. Roy. Meteor. Soc., 132, 585–603, doi:10.1256/qj.03.198.B, 2006.

Jöckel, P., von Kuhlmann, R., Lawrence, M., Steil, B., Brenninkmeijer, C., Crutzen, P., Rasch, P., and Eaton, B.: On a fundamental problem in implementing flux-form advection schemes for tracer transport in 3-dimensional general circulation and chemistry transport models, Q. J. Roy. Meteor. Soc., 127, 1035–1052, 2001.

Kawa, S., Erickson, D., Pawson, S., and Zhu, Z.: Global CO_2 transport simulations using meteorological data from the NASA data assimilation system, J. Geophys. Res., 109, doi:10.1029/2004JD004554, 2004.

Kobayashi, S., Ota, Y., Harada, Y., Ebita, A., Moriya, M., Onoda, H., Onogi, K., Kamahori, H., Kobayashi, C., Endo, H., Miyaoka, K., and Takahashi, K.: The JRA-55 Reanalysis: General Specifications and Basic Characteristics, J. Meteorol. Soc. Jpn., 93, 5–48, doi:10.2151/jmsj.2015-001, 2015.

Kodama, C., Terai, M., Noda, A., Yamada, Y., Satoh, M., Seiki, T., Iga, S.-I., Yashiro, H., Tomita, H., and Minami, K.: Scalable rank-mapping algorithm for an icosahedral grid system on the massive parallel computer with a 3-D torus network, Parallel Comput., 40, 362–373, doi:10.1016/j.parco.2014.06.002, 2014.

Krol, M., Houweling, S., Bregman, B., van den Broek, M., Segers, A., van Velthoven, P., Peters, W., Dentener, F., and Bergamaschi, P.: The two-way nested global chemistry-transport zoom model TM5: algorithm and applications, Atmos. Chem. Phys., 5, 417–432, doi:10.5194/acp-5-417-2005, 2005.

Le Quéré, C., Andrew, R. M., Canadell, J. G., Sitch, S., Korsbakken, J. I., Peters, G. P., Manning, A. C., Boden, T. A., Tans, P. P., Houghton, R. A., Keeling, R. F., Alin, S., Andrews, O. D., Anthoni, P., Barbero, L., Bopp, L., Chevallier, F., Chini, L. P., Ciais, P., Currie, K., Delire, C., Doney, S. C., Friedlingstein, P., Gkritzalis, T., Harris, I., Hauck, J., Haverd, V., Hoppema, M., Klein Goldewijk, K., Jain, A. K., Kato, E., Körtzinger, A., Landschützer, P., Lefèvre, N., Lenton, A., Lienert, S., Lombardozzi, D., Melton, J. R., Metzl, N., Millero, F., Monteiro, P. M. S., Munro, D. R., Nabel, J. E. M. S., Nakaoka, S.-I., O'Brien, K., Olsen, A., Omar, A. M., Ono, T., Pierrot, D., Poulter, B., Rödenbeck, C., Salisbury, J., Schuster, U., Schwinger, J., Séférian, R., Skjelvan, I., Stocker, B. D., Sutton, A. J., Takahashi, T., Tian, H., Tilbrook, B., van der Laan-Luijkx, I. T., van der Werf, G. R., Viovy, N., Walker, A. P., Wiltshire, A. J., and Zaehle, S.: Global Carbon Budget 2016, Earth Syst. Sci. Data, 8, 605–649, doi:10.5194/essd-8-605-2016, 2016.

Liu, J., Bowman, K., Lee, M., Henze, D., Bousserez, N., Brix, H., Collatz, G. J., Menemenlis, D., Ott, L., Pawson, S., Jones, D., and Nassar, R.: Carbon monitoring system flux estimation and attribution: impact of ACOS-GOSAT XCO_2 sampling on the inference of terrestrial biospheric sources and sinks, Tellus B, 66, 22486, doi:10.3402/tellusb.v66.22486, 2014.

Machida, T., Matsueda, H., Sawa, Y., Nakagawa, Y., Hirotani, K., Kondo, N., Goto, K., Nakazawa, T., Ishikawa, K., and Ogawa, T.: Worldwide Measurements of Atmospheric CO_2 and Other Trace Gas Species Using Commercial Airlines, J. Atmos. Ocean. Tech., 25, 1744–1754, doi:10.1175/2008JTECHA1082.1, 2008.

Matsueda, H., Machida, T., Sawa, Y., and Niwa, Y.: Long-term change of CO_2 latitudinal distribution in the upper troposphere, Geophys. Res. Lett., 42, 2508–2514, doi:10.1002/2014GL062768, 2015.

Meirink, J. F., Bergamaschi, P., Frankenberg, C., d'Amelio, M. T. S., Dlugokencky, E. J., Gatti, L. V., Houweling, S., Miller, J. B., Röckmann, T., Villani, M. G., and Krol, M. C.: Four-dimensional variational data assimilation for inverse modeling of atmospheric methane emissions: Analysis of SCIAMACHY observation, J. Geophys. Res., 113, doi:10.1029/2007JD009740, 2008.

Mellor, G. L. and Yamada, T.: A Hierarchy of Turbulence Closure Models for Planetary Boundary Layers, J. Atmos. Sci., 31, 1791–1806, 1974.

Miura, H.: An Upwind-Biased Conservative Advection Scheme for Spherical Hexagonal–Pentagonal Grids, Mon. Weather Rev., 135, 4038–4044, doi:10.1175/2007MWR2101.1, 2007.

Miura, H., Satoh, M., Nasuno, T., Noda, A. T., and Oouchi, K.: A Madden–Jullian Oscillation event simulated using a global cloud-resolving model, Science, 318, 1763–1765, 2007.

Miyakawa, T., Satoh, M., Miura, H., Tomita, H., Yashiro, H., Noda, A., Yamada, Y., Kodama, C., Kimoto, M., and Yoneyama, K.: Madden-Julian Oscillation prediction skill of a new-generation global model demonstrated using a supercomputer., Nat. Commun., 5, 3769, doi:10.1038/ncomms4769, 2014.

Miyamoto, Y., Kajikawa, Y., Yoshida, R., Yamaura, T., Yashiro, H., and Tomita, H.: Deep moist atmospheric convection in a subkilometer global simulation, Geophys. Res. Lett., 40, 4922–4926, doi:10.1002/grl.50944, 2013.

Nakanishi, M. and Niino, H.: An Improved Mellor–Yamada Level-3 Model with Condensation Physics: Its Design and Verification, Bound.-Lay. Meteorol., 112, 1–31, doi:10.1023/B:BOUN.0000020164.04146.98, 2004.

Niwa, Y., Patra, P. K., Sawa, Y., Machida, T., Matsueda, H., Belikov, D., Maki, T., Ikegami, M., Imasu, R., Maksyutov, S., Oda, T., Satoh, M., and Takigawa, M.: Three-dimensional variations of atmospheric CO_2: aircraft measurements and multi-transport model simulations, Atmos. Chem. Phys., 11, 13359-13375, doi:10.5194/acp-11-13359-2011, 2011a.

Niwa, Y., Tomita, H., Satoh, M., and Imasu, R.: A Three-Dimensional Icosahedral Grid Advection Scheme Preserving Monotonicity and Consistency with Continuity for Atmospheric Tracer Transport, J. Meteorol. Soc. Jpn., 89, 255–268, doi:10.2151/jmsj.2011-306, 2011b.

Niwa, Y., Machida, T., Sawa, Y., Matsueda, H., Schuck, T. J., Brenninkmeijer, C. A. M., Imasu, R., and Satoh, M.: Imposing strong constraints on tropical terrestrial CO_2 fluxes using passenger aircraft based measurements, J. Geophys. Res., 117, doi:10.1029/2012JD017474, 2012.

Niwa, Y., Fujii, Y., Sawa, Y., Iida, Y., Ito, A., Satoh, M., Imasu, R., Tsuboi, K., Matsueda, H., and Saigusa, N.: A 4D-Var inversion system based on the icosahedral grid model (NICAM-TM 4D-Var v1.0): 2. Optimization scheme and identical twin exper-

iment of atmospheric CO_2 inversion, Geosci. Model Dev. Discuss., doi:10.5194/gmd-2016-232, in review, 2016.

Noda, A. T., Oouchi, K., Satoh, M., Tomita, H., Iga, S.-i., and Tsushima, Y.: Importance of the subgrid-scale turbulent moist process: Cloud distribution in global cloud-resolving simulations, Atmos. Res., 96, 208–217, doi:10.1016/j.atmosres.2009.05.007, 2010.

Olsen, S. C. and Randerson, J. T.: Differences between surface and column atmospheric CO_2 and implications for carbon cycle research, J. Geophys. Res., 109, doi:10.1029/2003JD003968, 2004.

Onogi, K., Tsutsui, J., Koide, H., Sakamoto, M., Kobayashi, S., Hatsushika, H., Matsumoto, T., Yamazaki, N., Kamahori, H., Takahashi, K., Kadokura, S., Wada, K., Kato, K., Oyama, R., Ose, T., Mannoji, N., and Taira, R.: The JRA-25 Reanalysis, J. Meteorol. Soc. Jpn., 85, 369–432, doi:10.2151/jmsj.85.369, 2007.

Patra, P. K., Law, R. M., Peters, W., Rödenbeck, C., Takigawa, M., Aulagnier, C., Baker, I., Bergmann, D. J., Bousquet, P., Brandt, J., Bruhwiler, L., Cameron-Smith, P. J., Christensen, J. H., Delage, F., Denning, A. S., Fan, S., Geels, C., Houweling, S., Imasu, R., Karstens, U., Kawa, S. R., Kleist, J., Krol, M. C., Lin, S.-J., Lokupitiya, R., Maki, T., Maksyutov, S., Niwa, Y., Onishi, R., Parazoo, N., Pieterse, G., Rivier, L., Satoh, M., Serrar, S., Taguchi, S., Vautard, R., Vermeulen, A. T., and Zhu, Z.: TransCom model simulations of hourly atmospheric CO_2: Analysis of synoptic-scale variations for the period 2002–2003, Global Biogeochem. Cy., 22, doi:10.1029/2007GB003081, 2008.

Patra, P. K., Takigawa, M., Dutton, G. S., Uhse, K., Ishijima, K., Lintner, B. R., Miyazaki, K., and Elkins, J. W.: Transport mechanisms for synoptic, seasonal and interannual SF_6 variations and "age" of air in troposphere, Atmos. Chem. Phys., 9, 1209–1225, doi:10.5194/acp-9-1209-2009, 2009.

Patra, P. K., Houweling, S., Krol, M., Bousquet, P., Belikov, D., Bergmann, D., Bian, H., Cameron-Smith, P., Chipperfield, M. P., Corbin, K., Fortems-Cheiney, A., Fraser, A., Gloor, E., Hess, P., Ito, A., Kawa, S. R., Law, R. M., Loh, Z., Maksyutov, S., Meng, L., Palmer, P. I., Prinn, R. G., Rigby, M., Saito, R., and Wilson, C.: TransCom model simulations of CH_4 and related species: linking transport, surface flux and chemical loss with CH_4 variability in the troposphere and lower stratosphere, Atmos. Chem. Phys., 11, 12813–12837, doi:10.5194/acp-11-12813-2011, 2011.

Peylin, P., Law, R. M., Gurney, K. R., Chevallier, F., Jacobson, A. R., Maki, T., Niwa, Y., Patra, P. K., Peters, W., Rayner, P. J., Rödenbeck, C., van der Laan-Luijkx, I. T., and Zhang, X.: Global atmospheric carbon budget: results from an ensemble of atmospheric CO_2 inversions, Biogeosciences, 10, 6699–6720, doi:10.5194/bg-10-6699-2013, 2013.

Randerson, J. T., Thompson, M. V., Conway, T. J., Fung, I. Y., and Field, C. B.: The contribution of terrestrial sources and sinks to trends in the seasonal cycle of atmospheric carbon dioxide, Global Biogeochem. Cy., 11, 535–560, doi:10.1029/97GB02268, 1997.

Rödenbeck, C.: Estimating CO_2 sources and sinks from atmospheric mixing ratio measurements using a global inversion of atmospheric transport, Max-Planck-Institut für Biogeochemie: Technical Paper 6, 2005.

Sandu, A., Daescu, D. N., Carmichael, G. R., and Chai, T.: Adjoint sensitivity analysis of regional air quality models, J. Comput. Phys., 204, 222–252, doi:10.1016/j.jcp.2004.10.011, 2005.

Sasakawa, M., Shimoyama, K., Machida, T., Tsuda, N., Suto, H., Arshinov, M., Davydov, D., Fofonov, A., Krasnov, O., Saeki, T., Koyama, Y., and Maksyutov, S.: Continuous measurements of methane from a tower network over Siberia, Tellus B, 62, 403–416, doi:10.1111/j.1600-0889.2010.00494.x, 2010.

Satoh, M., Matsuno, T., Tomita, H., Miura, H., Nasuno, T., and Iga, S.: Nonhydrostatic icosahedral atmospheric model (NICAM) for global cloud resolving simulations, J. Comput. Phys., 227, 3486–3514, doi:10.1016/j.jcp.2007.02.006, 2008.

Satoh, M., Tomita, H., Yashiro, H., Miura, H., Kodama, C., Seiki, T., Noda, A. T., Yamada, Y., Goto, D., Sawada, M., Miyoshi, T., Niwa, Y., Hara, M., Ohno, T., Iga, S., Arakawa, T., Inoue, T., and Kubokawa, H.: The Non-hydrostatic Icosahedral Atmospheric Model: description and development, Progress in Earth and Planetary Science, 1, 1–32, doi:10.1186/s40645-014-0018-1, 2014.

Sawa, Y., Tanimoto, H., Yonemura, S., Matsueda, H., Wada, A., Taguchi, S., Hayasaka, T., Tsuruta, H., Tohjima, Y., Mukai, H., Kikuchi, N., Katagiri, S., and Tsuboi, K.: Widespread pollution events of carbon monoxide observed over the western North Pacific during the East Asian Regional Experiment (EAREX) 2005 campaign, J. Geophys. Res., 112, doi:10.1029/2006JD008055, 2007.

Sawa, Y., Machida, T., and Matsueda, H.: Seasonal variations of CO_2 near the tropopause observed by commercial aircraft, J. Geophys. Res., 113, doi:10.1029/2008JD010568, 2008.

Sawa, Y., Machida, T., Matsueda, H., Niwa, Y., Tsuboi, K., Murayama, S., Morimoto, S., and Aoki, S.: Seasonal changes of CO_2, CH_4, N_2O and SF_6 in the upper troposphere/lower stratosphere over the Eurasian continent observed by commercial airliner, Geophys. Res. Lett., 42, 2001–2008, doi:10.1002/2014GL062734, 2015.

Shirai, T., Machida, T., Matsueda, H., Sawa, Y., Niwa, Y., Maksyutov, S., and Higuchi, K.: Relative contribution of transport/surface flux to the seasonal vertical synoptic CO_2 variability in the troposphere over Narita, Tellus B, 64, 19138, doi:10.3402/tellusb.v64i0.19138, 2012.

Stohl, A., Cooper, O. R., and James, P.: A Cautionary Note on the Use of Meteorological Analysis Fields for Quantifying Atmospheric Mixing, J. Atmos. Sci., 61, 1446–1453, doi:10.1175/1520-0469(2004)061<1446:ACNOTU>2.0.CO;2, 2004.

Stuhne, G. and Peltier, W.: Vortex Erosion and Amalgamation in a New Model of Large Scale Flow on the Sphere, J. Comput. Phys., 128, 58–81, doi:10.1006/jcph.1996.0196, 1996.

Takahashi, T., Sutherland, S. C., Wanninkhof, R., Sweeney, C., Feely, R. A., Chipman, D. W., Hales, B., Friederich, G., Chavez, F., Sabine, C., Watson, A., Bakker, D. C., Schuster, U., Metzl, N., Yoshikawa-Inoue, H., Ishii, M., Midorikawa, T., Nojiri, Y., Körtzinger, A., Steinhoff, T., Hoppema, M., Olafsson, J., Arnarson, T. S., Tilbrook, B., Johannessen, T., Olsen, A., Bellerby, R., Wong, C., Delille, B., Bates, N., and de Baar, H. J.: Climatological mean and decadal change in surface ocean pCO_2, and net sea-air CO_2 flux over the global oceans, Deep-Sea Res. Pt. II, 56, 554–577, 2009.

Thuburn, J.: Multidimensional Flux-Limited Advection Schemes, J. Comput. Phys., 123, 74–83, doi:10.1006/jcph.1996.0006, 1996.

Thuburn, J. and Haine, T. W. N.: Adjoints of Nonoscillatory Advection Schemes, J. Comput. Phys., 171, 616–631, doi:10.1006/jcph.2001.6799, 2001.

Tomita, H.: A Stretched Icosahedral Grid by a New Grid Transformation, J. Meteorol. Soc. Jpn., 86A, 107–119, doi:10.2151/jmsj.86A.107, 2008.

Tomita, H. and Satoh, M.: A new dynamical framework of nonhydrostatic global model using the icosahedral grid, Fluid Dyn. Res., 34, 357–400, doi:10.1016/j.fluiddyn.2004.03.003, 2004.

Tomita, H., Goto, K., and Satoh, M.: A New Approach to Atmospheric General Circulation Model: Global Cloud Resolving Model NICAM and its Computational Performance, Siam J. Sci. Comput., 30, 2755–2776, doi:10.1137/070692273, 2008.

van der Werf, G. R., Randerson, J. T., Giglio, L., Collatz, G. J., Mu, M., Kasibhatla, P. S., Morton, D. C., DeFries, R. S., Jin, Y., and van Leeuwen, T. T.: Global fire emissions and the contribution of deforestation, savanna, forest, agricultural, and peat fires (1997–2009), Atmos. Chem. Phys., 10, 11707–11735, doi:10.5194/acp-10-11707-2010, 2010.

Vukićević, T. and Hess, P.: Analysis of tropospheric transport in the Pacific Basin using the adjoint technique, J. Geophys. Res., 105, 7213–7230, doi:10.1029/1999JD901110, 2000.

Vukićević, T., Steyskal, M., and Hecht, M.: Properties of Advection Algorithms in the Context of Variational Data Assimilation, Mon. Weather Rev., 129, 1221–1231, doi:10.1175/1520-0493(2001)129<1221:POAAIT>2.0.CO;2, 2001.

Wada, A., Matsueda, H., Sawa, Y., Tsuboi, K., and Okubo, S.: Seasonal variation of enhancement ratios of trace gases observed over 10 years in the western North Pacific, Atmos. Environ., 45, 2129–2137, doi:10.1016/j.atmosenv.2011.01.043, 2011.

Wilson, C., Chipperfield, M. P., Gloor, M., and Chevallier, F.: Development of a variational flux inversion system (INVICAT v1.0) using the TOMCAT chemical transport model, Geosci. Model Dev., 7, 2485–2500, doi:10.5194/gmd-7-2485-2014, 2014.

Yokota, T., Yoshida, Y., Eguchi, N., Ota, Y., Tanaka, T., Watanabe, H., and Maksyutov, S.: Global Concentrations of CO_2 and CH_4 Retrieved from GOSAT: First Preliminary Results, SOLA, 5, 160–163, doi:10.2151/sola.2009-041, 2009.

Yumimoto, K. and Takemura, T.: The SPRINTARS version 3.80/4D-Var data assimilation system: development and inversion experiments based on the observing system simulation experiment framework, Geosci. Model Dev., 6, 2005–2022, doi:10.5194/gmd-6-2005-2013, 2013.